

Modeling wind load paths and sharing in a wood-frame building

Jing He¹, Fang Pan² and C.S. Cai^{*1}

¹Department of Civil and Environmental Engineering, Louisiana State University, Baton Rouge, LA 70803, USA

²Southwest Research Institute, San Antonio, TX 78228, USA

(Received March 31, 2018, Revised July 13, 2018, Accepted September 11, 2018)

Abstract. While establishing adequate load paths in the light-frame wood structures is critical to maintain the overall structural integrity and avoid significant damage under extreme wind events, the understanding of the load paths is limited by the high redundant nature of this building type. The objective of the current study is to evaluate the system effects and investigate the load paths in the wood structures especially the older buildings for a better performance assessment of the existing building stock under high winds, which will provide guidance for building constructions in the future. This is done by developing building models with configurations that are suspicious to induce failure per post damage reconnaissance. The effect of each configuration to the structural integrity is evaluated by the first failure wind speed, a major indicator beyond the linear to the nonlinear range. A 3D finite-element (FE) building model is adopted as a control case that is modeled using a validated methodology in a highly-detailed fashion where the nonlinearity of connections is explicitly simulated. This model is then altered systematically to analyze the effects of configuration variations in the model such as the gable end sheathing continuity and the gable end truss stiffness, etc. The resolution of the wind loads from scaled wind tunnel tests is also discussed by comparing the effects to wind loads derived from large-scale wind tests.

Keywords: residential buildings; load paths; load sharing; wind loads; finite element

1. Introduction

The light-frame wood buildings in the U.S. account for over 95% of all the residential structures most of which are designed as low-rise buildings (Fischer and Kasal 2009). For the U.S. population, around one-third resides within 100 miles of hurricane-prone coastline by 2007, i.e., the Atlantic and Gulf coasts (US Census Bureau 2007). Meanwhile, the population in coastline areas grows steadily, i.e., from 47 million in 1960 to 87 million in 2008 (Wilson and Fischetti, 2010), putting their residential houses in great danger. As a result, the residential light-frame wood houses become the major source of the monetary losses caused by the extreme wind events, e.g., approximately 60% of the total insured losses for Hurricane Hugo (Sparks 1991).

Observations from the reconnaissance trips on the wind damage events revealed that the main source of damage in houses was the lack of continuous uplift load path from the roof down to the foundation to resist uplift winds (van de Lindt *et al.* 2007), where the most common failure is concentrated on the roof sheathing and connections (Dijkers *et al.* 1970, van de Lindt *et al.* 2007). Such poor performance is likely the result of some factors. First, most residential buildings in the U.S. are conventional, non-engineered (or called deemed-to-comply) construction where the construction techniques are based on tradition and experience with little solid engineering input, especially under wind loads for these critical members. Second, the older house stock typically suffered more damage due to the

insufficient building codes in terms of the anchor spacing and wind loads, etc. For example, the older homes in Florida built to the old code SBC experienced more damage in Hurricane Charley than the buildings constructed since the adoption of 2001 FBC (FEMA 2005). Third, the misconstruction due to the poor inspections such as the missing nails and the degradation of the building component and connections resulted from the material deterioration and termite infestation, etc. lead to the weaknesses in the uplift load paths.

As stated above, one interesting phenomenon that has been repeatedly documented is that while the newly built houses perform relatively well during hurricanes with little to no damage to the structural system, for the older buildings, damage observations are pervasive due to the insufficient design and construction of old codes as shown in Fig. 1 (e.g., FEMA 2005, 2006, van de Lindt *et al.* 2007). Such vulnerability and potential damage in the large portion of existing old building stock aroused our attention, and there is an urgent need to investigate how the load shares and distributes in the building configuration that tends to induce failure in both qualitative and quantitative ways.

When the wind blows onto a building, uplift pressures could develop on the roof surface due to the flow separation at the leading edges, i.e., the top of the windward wall and the roof ridge. These loads will be distributed on the sheathing panels which then send the loads to the truss assemblies through the sheathing-to-truss connections (STTCs) such as sheathing nails. These loads on the truss assemblies will be further transferred to the walls via the toe-nails or metal straps, generally referred to as the roof-to-wall connections (RTWCs) that link the truss top chord to the top plate of the wall. In the end, the loads flow along the

*Corresponding author, Professor
E-mail: cscai@lsu.edu

wall studs and reach the foundation through the connections such as foundation hold-downs or anchor bolts. The current consensus on the load path and the load sharing is twofold: structural loads tend to follow the path of greatest resistance in terms of the stiffness (Wolfe and McCarthy 1989), which thus carries a greater share of loads; the load sharing increases the capacity of individual member by distributing loads to adjacent members (Wolfe and LaBissoniere 1991). However, the indeterminate light-frame wood structure that is made of repetitive frame members is highly redundant. This limits the understanding on how the loads share and distribute through numerous possible load paths in different configurations under the complex wind loading condition.

In light of this, a comprehensive study on the system behavior of and the load paths in the light-frame wood structures is imperative and is the objective of the current study to improve their performance and mitigate their failure to strong winds. The scope of the current study covers a wide range of parameters that can affect the damage of houses as indicated by FEMA (2005), including the gable end sheathing continuity, the gable end truss stiffness, the STTC schedule, the opening condition, and the sheathing thickness. The effects of these different building configurations on the building performance are analyzed with the aid of a validated 3D nonlinear finite-element (FE) model and are directly evaluated in the failure stage that goes from the material linear to the nonlinear range by the first failure wind speed. The resolution of wind loads provided by the wind tunnel tests on small-scale building models is also discussed by comparing the wind effects to that of the loads derived from large-scale wind tests. The results of these investigations serve a better estimation on the performance of the existing building stock under high winds, enable the application of proper mitigation techniques, and provide guidance for the future constructions.



Fig. 1 Newer building with little damage and older building in the same neighborhood with extensive structural damages after Hurricane Katrina (van de Lindt *et al.* 2007)

2. Literature review

Martin *et al.* (2011) developed a full 3D linear rectangular building model where connections at the foundation were modeled as linear spring elements to account for the load-displacement behavior. Other connections such as the sheathing nails and RTWCs were simplified as rigidly connected, and the effect of nail spacing was simply incorporated by adjusting the shear modulus of sheathing. Two geometric scenarios were investigated by this model to evaluate system effects and explore the load paths under uniform uplift pressures. The edge nailing of the wall sheathing (2, 3, 4, 6, 12-in spacing considered) was revealed to affect the distribution of loads from the roof to foundation, especially the nailing on the gable wall where the denser the edge nailing gets, the more evenly the loads distribute to the foundation. For the wall opening effects, it was found the load carrying capacity for the entire wall would drop due to the occurrence of opening, and the wall opposite to the opening can also be influenced dependent on the orientation of the related trusses. However, the effects of the considered scenarios were only checked on the foundation level since the foundation hold-downs and anchor bolts were the only connections explicitly represented with finite elements where the loads carried can be examined more accurately. In addition, this linear model cannot reflect load redistributions due to the nonlinear behavior of the critical components such as sheathing nails and RTWCs of a light-frame wood building under uplift loads.

This simplified linear modeling methods developed by Martin *et al.* (2011) was later adopted by Pfretzschner *et al.* (2014) and Malone *et al.* (2013). Pfretzschner *et al.* (2014) expanded its application to a more complex L-shaped wood house to investigate the effects of reentrant corners, wall openings, and gable-end retrofits on load paths. The effect of adding the reentrant corner or the opening was found to be largely dependent on the orientation of trusses with respect to the walls. The large torsion induced by the reentrant corners might be reduced by balancing the stiffness of the walls. Openings in the wall parallel to the trusses had the least effect on the uplift reactions in the remaining walls. Effects of the retrofit were examined and showed no signs of additional torsion by modeling C-shaped retrofit at each of the gable-end studs. Malone *et al.* (2013) took the perspective of highlighting the difference in the load paths between the timber frame (TF) and the light-frame (LF) structure. The TF was found superior to the LF in resisting both uplift and story drift because the continuous posts resisted the out-of-plane wind loadings more effectively than the platform-framed exterior walls did, and the structural insulated panels used in the TF had greater stiffness compared with the LF shear walls. However, based on the same modeling methods, Pfretzschner *et al.* (2014) and Malone *et al.* (2013)'s investigation on the load paths were also limited to elastic range as concluded by Martin *et al.* (2011), and the nonlinear behavior of the critical members such as the sheathing nails cannot be captured.

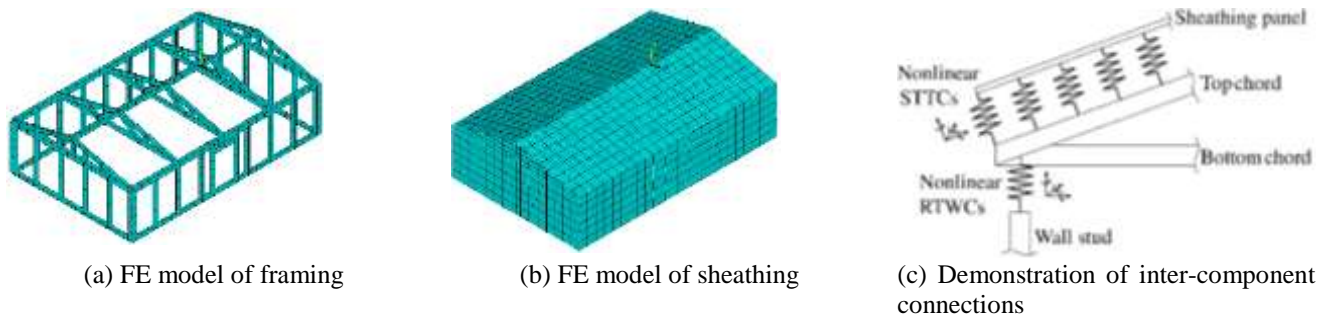


Fig. 2 Building model

The modeling resolution has generally been improved at the assembly and the component level, e.g., the roof structure and RTWCs. Shivarudrappa and Nielson (2013) developed a roof structure model where STTCs and RTWCs are explicitly modeled with nonlinear spring elements. Sensitivity studies were performed to investigate the uplift load paths in both the linear and nonlinear range by load influence coefficient contours under point loads on parameters such as the connection stiffness, sheathing stiffness, framing type, and nonlinear behavior. For the RTWCs, the load paths were found more sensitive to the overall stiffness, and their relative stiffness began to have larger impacts when they entered the nonlinear range with decreased stiffness. Compared with sheathing connections, sheathing stiffness itself had a notable impact on the load distribution. However, such a modeling on the roof assemblies only reflects a part of the entire load paths from the roof to foundation, and these load paths may shift with the load redistribution due to the neglect of the interaction with the wall system, causing the discrepancies with the real case. Aiming at the modeling resolution of the RTWCs, Satheeskumar *et al.* (2016) developed a solid model of the roof-to-wall triple grip connection that consisted of five separate parts: triple grip, nail, membrane, truss, and top plate. This model accounts for the large deformation and the contact between the nail and timber in linear and nonlinear phases up to failure. Load paths on this scale were found to be significantly affected by the nails located near the centerline of the loading action in that the responses of these nails dominated the uplift capacity and failure types of the RTWCs. The verification of this model against test results showed the predictions given by the FE model were acceptable in terms of the deformation and the failure mode. The force-displacement relationship obtained from this model could be used as a substitution of experimental measurements. The challenge with such a model is how to incorporate this relationship into a 3D full building model.

Besides the effect of FE model techniques used, load paths and sharing in the wood house under extreme wind events are also dependent on the resolution of loading. The current loading forms include the uplift uniform pressures, the wind codes defined values (e.g., ASCE 7-10), discretized static pressures, and database-assisted design (DAD) time-history pressures (He *et al.* 2017). The uplift uniform pressure is the most simplified version, which qualitatively represents the characteristics of wind loads

that induce suctions (uplift force) on the roof (e.g., Martin *et al.* 2011, Shivarudrappa and Nielson 2013, Pfretzschner *et al.* 2014). This form is easy to apply and convenient to do sensitivity studies but cannot reflect the true wind loading distribution. As oppose to that, other forms are quantitatively based utilizing the wind pressures measured from wind tunnels or other tools. Among these forms, the wind provisions in codes are of the lowest resolution providing pressure coefficients in prescribed zones with peak values derived from wind tunnel tests (e.g., Asiz *et al.* 2009, Malone *et al.* 2013, He *et al.* 2018a). To improve the accuracy of loads from provisions, many research adopted the similar procedure used in the development of the wind provisions to process the measured data but with finer area-averaged discretization (e.g., Cope 2004, Pan *et al.* 2014, He *et al.* 2017; 2018b). The modern experimental and computational techniques make possible to use the pressure time histories directly by the DAD method. Utilizing the pressures with spatial and temporal variations enable engineers to do transient dynamic analysis and to manipulate data into any target forms, such as peak values or mean values (e.g., Mensah *et al.* 2011, Roueche *et al.* 2015). However, the existing DAD databases are developed upon the wind tunnel tests on small-scale models. The discrepancies in the load paths under the wind tunnel pressure measurements with that under the field test loading is unknown. Thus, explorations on the effect of the wind loading resolution on the building performance are still needed.

3. Modeling methods and loading sources

3.1 Model description and modelling methods

A nonlinear numerical building model at an entire building scope developed by a validated modeling methodology (He *et al.* 2018b) is used in the current study to explore the factors that affect the vulnerability of the light-frame wood buildings under extreme wind events. The footprint dimensions of the numerical model are 2.19 m (7.2 ft) wide by 3.42 m (11.25 ft) long for an eave height of 0.79 m (2.6 ft), as shown in Fig. 2. It is a one-story gable roof wood house with a roof slope of 14° . The modeling methodology adopted is practical for users by directly employing the built-in features of the FE software,

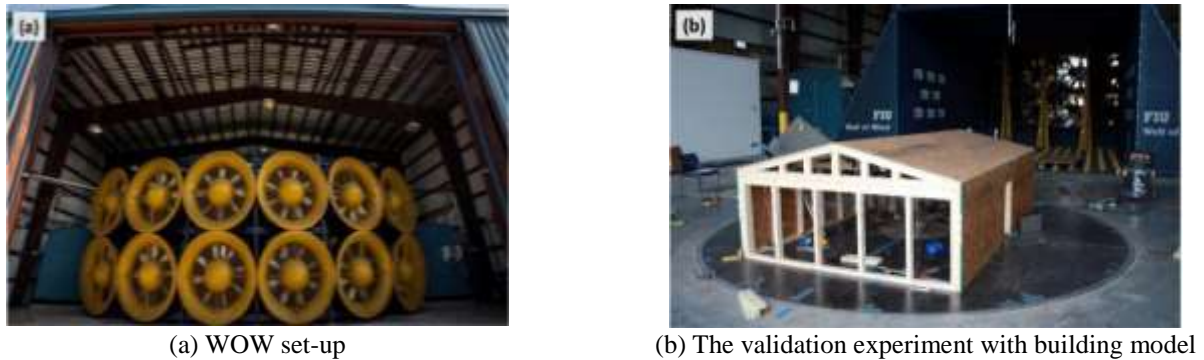


Fig. 3 FIU open-jet wind tests

Mechanical APDL (ANSYS), i.e., the beam members in the truss and wall are modeled by using beam elements, and the sheathings on the wall and roof are represented by shell elements.

This building including both the main frame and building envelope systems was modeled in great detail. Reflecting the performance of the most vulnerable components in the wood structure under uplift wind loads, inter-component connections including the sheathing nails and the RTWCs are modeled by nonlinear spring elements. Each spring element composed of two coincident nodes at the same location accounts for the behavior of the connection in each DOF in nodal directions. The multi-linear force-displacement relationship for each DOF is applied to the corresponding spring element that is consistent with the value used by He *et al.* (2018b). In order to accurately determine the location of each spring element and keep track of the node numbers of all the spring elements, the direct generation method is adopted for this modeling technique. To capture the complex structural responses while maintaining the simplicity of the modeling technique, some assumptions are made. The material properties of the beam and sheathing wood members are assumed to be elastic isotropic and elastic orthotropic, respectively; the truss assembly is rigid connected at the heel and pinned connected for the rest; no internal compartment is considered, etc. Specific modeling features and detailed geometry of the building can be found in He *et al.* (2018b).

3.2 Model validation and FIU open-jet wind test datasets

The currently discussed building model was tested at the Wall of Wind (WOW) Experimental Facility (EF) at Florida International University (FIU), shown in Fig. 3. It was carried out to validate the nonlinear modeling methodology adopted and explore the failure modes as well as the progressive damages of residential houses under extreme wind events. The wind loads including the external and internal pressures were collected under a wind speed of 29.06 m/s (65 mph) under the wind directions varying from 0° to 180° with 15° intervals, considering symmetry of the building, for both the building model with and without door opening. Then, the wind speed was increased to 40.68 m/s

(91 mph) and 46.94 m/s (105 mph) with the same incident angles without door opening. The failure occurred in the mode of the STTC and roof sheathing panel under the 46.94 m/s (105 mph) speed wind with the direction of 75°. Please find He *et al.* (2018c) for more information about failure analysis. This direction of vulnerability is used throughout the current study. To maintain a higher resolution of the applied pressures, the loading grid is determined directly by the number of pressure taps. That is to say, the loading is discretized into 352 areas on the building surface corresponding to the 352 external pressure taps in total, and each pressure trace is used onto its equivalent areas without further area averaging so as to reflect all the fluctuations as measured by the pressure taps. Additional details can be found in He *et al.* (2018b). These wind load datasets with realistic pressure distributions are applied for the analysis of load paths and sharing.

3.3 NIST wind tunnel database

A wind load dataset on a 1/100 scaled building model from NIST aerodynamic database contributed by the Boundary Layer Wind Tunnel Laboratory at the University of Western Ontario (UWO) is applied as to verify the effect of scale relaxation and the resolution of the atmospheric boundary layer (ABL) simulated by scaled wind tunnel tests. Full-scale wind tests are irreplaceable due to the incompatible similarity issues associated with the ABL physical modeling in wind tunnels such as the duplication of the Reynolds number, raising studies on the subject of the smallest model scaling of a low-rise building in wind tunnels, i.e., 1:50 recommended by Tieleman (2003). The Reynolds number effects also lead to the discrepancies in the peak pressure coefficients between the wind tunnel simulation and full-scale wind tests. Specifically, the peak pressure is determined by the turbulence intensity and the power spectrum density of the free stream where the small-scale turbulence is important for the roll-up of the separated shear layer, and the large-scale turbulence is responsible for the vortices to reach full maturity (Tieleman 1996, 2003, Ahmad and Kumar 2002, Ho *et al.* 2005). However, full-scale or large-scale wind tests are still in short. It is practical to utilize the available large amount of wind tunnel data sets, especially the aerodynamic databases such as NIST and Tokyo Polytechnic University (TPU) database that are

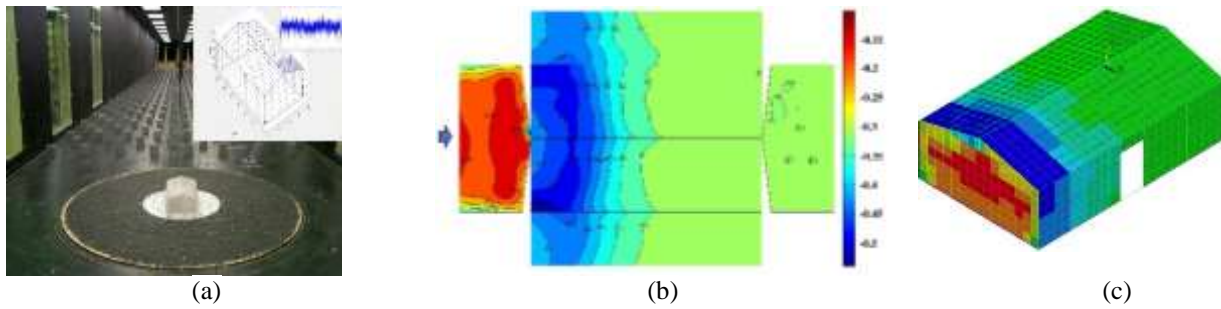


Fig. 4 NIST dataset: (a) 80 ft *125 ft *32 ft model and its tap layout with direction instruction and a sample of Cp time history, (b) mean Cp contour ($\theta=180^\circ$) and (c) discretized mean Cp applied on the FE model ($\theta=180^\circ$)

Table 1 Scenarios used for the parameter study

Case	Gable sheathing continuity		Gable end truss stiffness			STTC schedule (in.)			Opening		Sheathing thickness (in.)			Load applied			
	1 Piece	2 Pieces	Fink	Gable	Queen	6/6	6/12	6(36)/12	w/o(a)	with	w/o(b)	7/16	23/32	7/8	FIU	NIST	Uniform
1	√			√					√			√			√		
2		√		√					√			√			√		
3	√		√						√			√			√		
4	√				√				√			√			√		
5	√			√		√			√			√			√		
6	√			√				√	√			√			√		
7	√			√						√		√			√		
8	√			√							√	√			√		
9	√			√					√				√		√		
10	√			√					√					√	√		
11	√			√					√			√				√	
12	√			√					√			√					√

serving for the database assisted design (DAD). Another look at the resolution of the wind tunnel data is taken from the perspective of structural response that is directly related to the response of structure rather than wind pressures. The average form of wind loads instead of the peak values is used for the current study due to its high correlation between wind tunnel simulation and full-scale wind loads.

To be consistent with the FIU test, the selected data set is for the low-rise, gable roof building in open terrain (roughness length, $z_0=0.03$ m). The geometries of the two building models are similar in the roof slope (14°) and the aspects ratio (length: width: roof height), i.e., $38.1\text{ m} \times 24.4\text{ m} \times 9.75\text{ m}$ (125 ft. \times 80 ft. \times 32 ft.) of the NIST model and $3.5\text{ m} \times 2.3\text{ m} \times 0.91\text{ m}$ (11.72 ft. \times 7.5 ft. \times 3.0 ft.) of the FIU model, with variation only in size, which is approximately 10.7 to 1. As indicated by Ho *et al.* (2005), the mean pressure distributions on the buildings with an identical aspect ratio can reach quite well agreements with slightly lower values on building with lower eave heights due to the difference in the characteristics of the turbulence at different height. Hence, the mean values of pressure coefficient data measured from total 625 taps on the model in the UWO wind tunnel experiment are adopted and the noteworthy that the pressure distribution measurement has

taken account of the internal pressure due to the distributed leakage. A demonstration of the derived mean Cp contour and its distribution on the FE model after discretization under the wind parallel to the ridge are shown in Fig. 4(c) and 4(d), respectively.

4. Load distribution parameter study

4.1 Geometric and loading scenarios

For the following load paths investigation, the Case 1 building model is set as the control case that is made up of conventional configurations as listed in Table 1. Then, this model is altered systematically in configurations and loading forms to perform parameter studies including the gable end sheathing continuity, gable end truss stiffness, STTC schedule, opening condition, sheathing thickness, and the loading resolution. A detailed description of parameters used in each case can be found in Table 1.

Cases 1 and 2 investigate the effect of gable end sheathing continuity on the load paths and building integrity. In the Case 2 model, the two-piece gable end sheathings are connected to the frame with the same conventional nailing

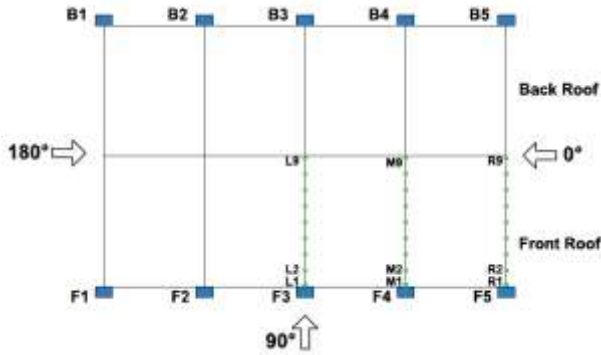


Fig. 5 Plan view of roof sheathing panels with connected frames showing the locations of RTWCs (blue square symbols) and STTCs (green circle symbols) (F=front, B=back, L=left, R=right, M=middle)

schedule as adopted in Case 1, i.e., 6 in. /12 in. along the exterior panel edge (edge nailing) and the intermediate supports (field nailing), respectively. Three conventional gable end truss types are discussed in Cases 1, 3, and 4 including the fink, gable, and queen type that have the similar web numbers but vary in the web configurations. Cases 1, 5, and 6 vary in the STTC schedule, of which the 6/6 and 6/12 nailing correspond to the new and old building code, respectively. The schedule 6(36)/12 here is defined as being consistent with that of the FIU wind test model which adopted 6/12 nailing except that the STTCs along the side walls intentionally set as 36 in. to weaken the load path. The changing in the stiffness of walls and the load paths resulted from adding opening is discussed in Cases 1, 7, and 8, in which the model has closed door, open door, and no door, respectively. The sheathing thicknesses considered correspond to the common OSB sheathing panels in the market, as shown in Cases 1, 9, and 10. The wind loading resolutions from different sources are examined in Cases 1, 11, and 12.

The effects of these parameters on the load paths under 100 mph wind are displayed by von Mises (VM) stress. It is an equivalent stress combining the stresses in all three directions into a single index that gives an appreciation of the overall magnitude of the tensor, and it is often used as an indicator of the failure by ductile tearing. Under the same wind speed, the structural response at the critical members shown in Fig. 5, including the RTWCs of the building model and the STTCs of the front roof sheathing panel on the right, provide another way of looking at the load distribution under the systematically changing parameters.

4.2 Failure threshold

The first failure wind speed and location are chosen as the final indices to reflect the effect of parameters discussed. The wind speed increases at an interval of 1 mph until failure. The STTC withdrawal failure is the only threshold considered as it is the dominant failure mode as witnessed in the past due to its relative lower capacity than the other connections, and therefore, it is efficient to use it to reflect

the first failure condition. Allowing for the time accumulation effects, the failure criteria of the sheathing nail are chosen as the withdrawal force reaching its capacity (680N) (Dao et al. 2008) rather than the nail exceeding a relative displacement representing the complete pullout.

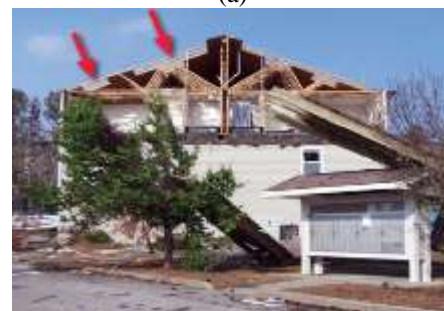
4.3 Effect of gable end sheathing continuity

The loss of sheathing on the gable end walls is a common failure observed in the past reconnaissance of wind damage, as shown in Fig. 6. The failure of the vulnerable gable end wall often leads to the pressurization and the complete collapse of the side of the structure. The purpose of this section is to investigate the effect of the gable end sheathing continuity on the sheathing behavior and the structural integrity as well as the load sharing on the critical connections. As stated above, since the Cases 1 and 2 models are installed with the one-piece and two-piece gable end sheathing, respectively, with the same nailing schedule, the difference between the two models is twofold: Case 2 model has one more piece of sheathing and one more line of edge nailing.

The general difference caused by the gable end sheathing continuity is displayed by VM stresses of wall sheathings on the gable and the building corner in Fig. 7. The Case 1 model with one-piece gable walls shows a stress concentration right beneath the roof ridge on both the gable end sheathings in Figs. 7(a) and 7(b). As opposed to that, the load is more evenly distributed by the two-piece gable sheathing model, i.e., the Case 2 model, with the smaller nailing tributary areas under the same loading condition.



(a)



(b)

Fig. 6 Gable end wall failure: (a) Hurricane Charley (FEMA 2005) and (b) Hurricane Katrina (FEMA 2006)

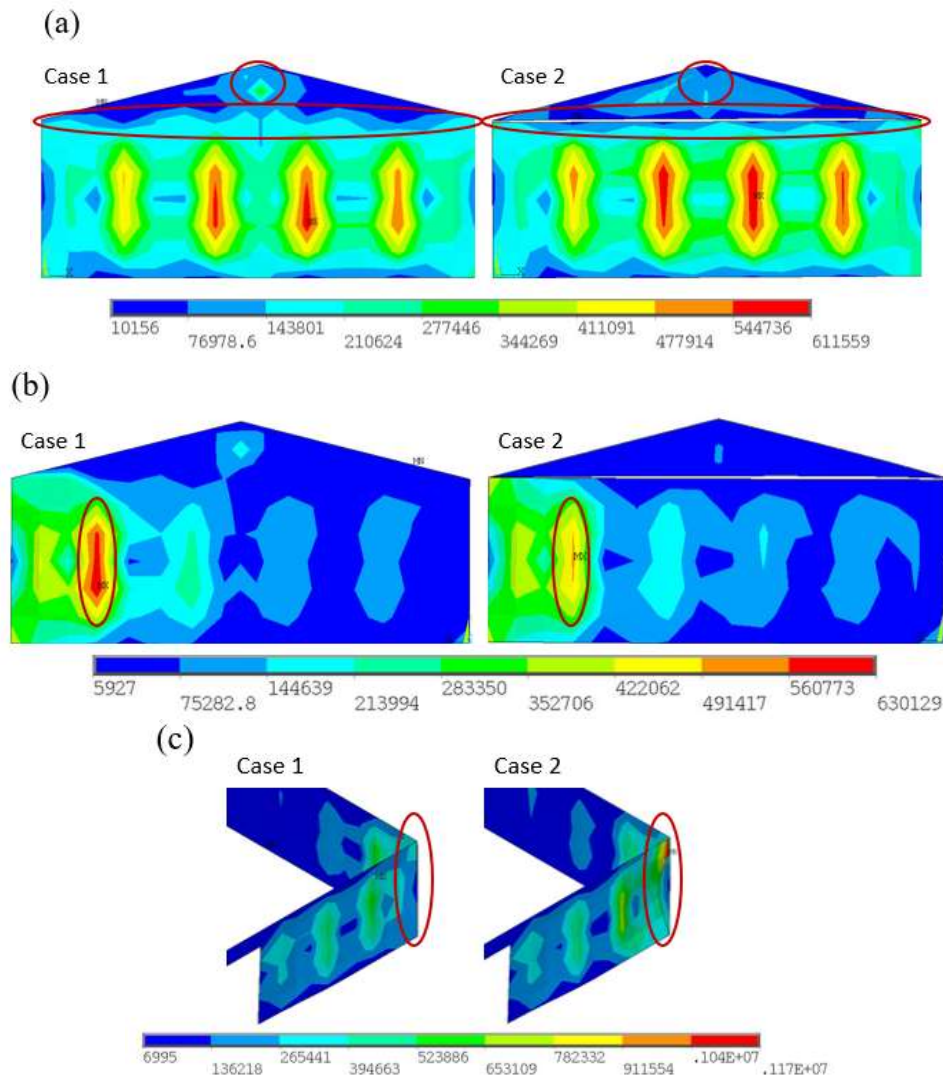


Fig. 7 VM comparison of gable wall sheathing continuity: (a) left wall (deformation scaler=100), (b) right wall (deformation scaler=100) and (c) windward corner (deformation scaler=40). Unit: N/m^2

For the sheathing area below the eave height, the Case 1 model experiences higher reactions on the right end wall, with the maximum increased by 19.48% occurring around the field nailing at a lower height compared with that of Case 2 due to the direct interactions with wind on the triangle areas. On the other hand, the stresses on the left end wall which is also mainly subjected to suction wind loads, are slightly higher in Case 2 model with the maximum increased by 1.98% (from 599418 N/m^2 to 611559 N/m^2).

In looking at the front wall on the corner in Fig. 7(c), the stress concentration and deformation are higher in Case 2 in response to the sacrifice of the structural integrity by breaking up the load path on the gable wall. However, since the front wall is not as vulnerable as the gable end walls or the roof assemblies, this weakness caused by the sheathing discontinuity is not significant.

Fig. 8 shows the withdrawal forces of the gable end sheathing nails at the bottom chord where the sheathing discontinuity is discussed. In the figure, Case 2_Up, Case 2_Down, and Case 2_Sum refers to the force of the Up nail

schedule, the Down nail schedule, and the summation of the Up and Down nail schedules, respectively. As the nailing gets denser, the wall would become stiffer and capable of distributing the wind loads more evenly through its sheathing nails, e.g., Case 1(105.58 N_2 variance) vs. Case 2_Sum (22.16 N_2 variance) for the right wall. As expected, with fewer nails, each sheathing nail in Case 1 carries more loads than the corresponding edge nailing in Case 2 on each of the two sheathing panels under the same wind loading. The maximum withdrawal force of Case 1 reaching 30.19 N on nail #6 of the left wall is higher than the maximum force (13.8 N) acting on the Case 2 sheathing nails which occurs at the same location, i.e., 54.3% reduction. The total summation forces carried by the sheathing nail at eave height in Case 1 (285.6 N) are also larger than the that in Case 2 (235.6 N). The practical implication of this finding is that even with the sacrifice of the sheathing continuity, installing more sheathing nails may increase the structural resistance to winds.

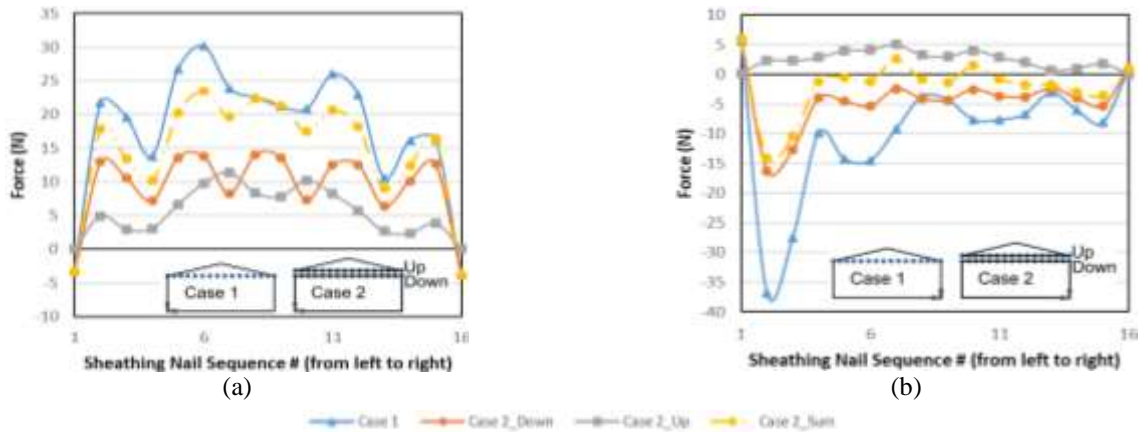


Fig. 8 Withdrawal force of gable sheathing nails at the bottom chord: (a) left wall and (b) right wall

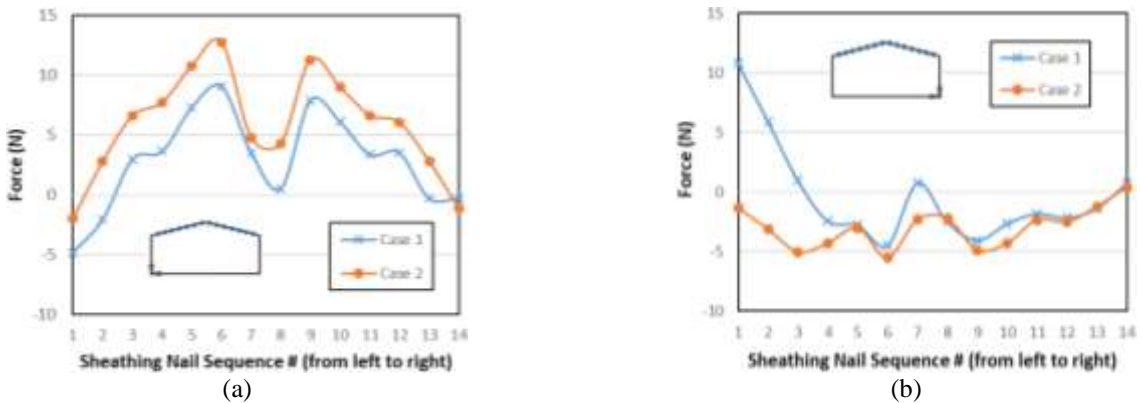


Fig. 9 Withdrawal force of gable sheathing nails at top chord: (a) left wall; (b) right wall

As the sheathing discontinuity breaks up the original load paths in Case 1, the loads redistribute and lead to the change in the direction of forces acting on the sheathing nails in Case 2. On the left wall in Fig. 8(a), the Case 1 sheathing nails at the eave height are in tension except the ones at the two ends, i.e., #1 and #16; while in Case 2, these two sheathing nails on the upper gable sheathing panel are also under tension. A similar trend is also observed on the right end wall in Fig. 8(b). The Case 1 nails are under compression except the two at each end, i.e., #1 and #16, and the corresponding nails in Case 2 connected to the lower sheathing follow the same rule. However, all the eave height sheathing nails connected to the upper sheathing panel in Case 2 are in tension. The negative force on the right wall nails is largely caused by the influence from the global building frame deformation. The positive force on the sheathing nails of the upper gable sheathing panel in Case 2 is primarily governed by the action of the local wind pressures and affected less by the interaction with the main wind resisting system after breaking up the sheathing continuity.

The withdrawal forces in sheathing nails at the top chord are shown in Fig. 9. The forces acting on Case 2 sheathing nails are in the similar range (0 N -15 N) of that on the sheathing nails connected to the bottom chord. With smaller

tributary area, the forces are more evenly distributed on the upper sheathing panel in Case 2. The overall absolute forces are larger in Case 2 for the left wall and in Case 1 for the right wall, which is consistent with the stress concentration results discussed above. Exceptions are on the #1 sheathing nails on both the end walls that have larger absolute forces in Case 1. The negative force representing the nail enduring a compression induces neither the nail shank withdrawal from the lumber nor the nail head pull-through of the sheathing panel, and thus can be ignored when considering failure. For the positive values, the sheathing nail receives its maximum of 12.7 N on the #6 nail of the left wall which is still way smaller than the peak value on the eave height, indicating that Case 1 model is more vulnerable on the gable end based on sheathing nails discussed. Additionally, the sheathing nails connected to the bottom chord are more vulnerable than the nails connected to the top chords.

The plots in Fig. 10 provide another way of looking at the structural stability influenced by the sheathing continuity at the gable ends subjected to wind loads. The uplift load distribution on the RTWCs including the five connectors on the back roof marked as B and the five connectors on the front roof denoted as F is considered. In Case 1, the uplift forces transferred to the connectors at the end trusses, i.e., B1, B5, F1, F5, are less than their

Table 2 Gable end truss type and its component (Case number is defined in Table 1)

	Case 1	Case 3	Case 4
Truss shape	Gable	Fink	Queen
Web	5	4	3
Web sheathing nail	1	0	1

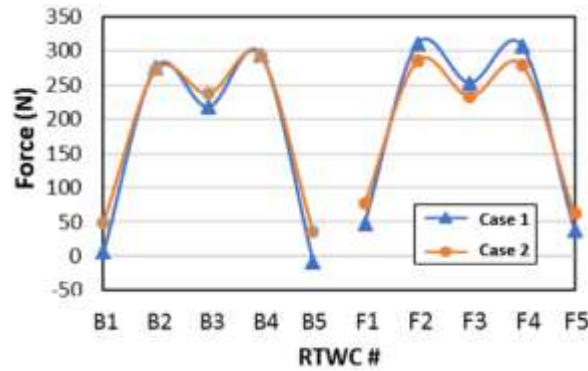


Fig. 10 Uplift force on RTWCs

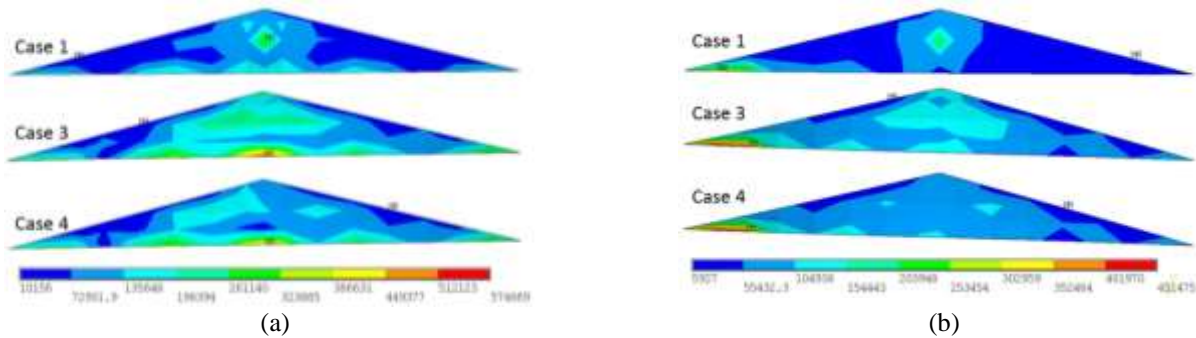


Fig. 11 VM comparison between truss shapes: (a) left gable sheathing (deformation scaler=200) and (b) right gable sheathing (deformation scaler=355)

counterparts in Case 2. Close investigation of this phenomenon reveals that this difference is induced by the contribution of the shear force provided by the sheathing nails at the gable end in Case 1 model. As the gable end sheathing continuously past the RTWCs and connected to the wall below, the shear force of the nails on the sheathing panels provides additional uplift connections between the roof assemblies and the walls. Thus, the load share taken by the RTWCs would decrease accordingly. The RTWCs in Case 1 take approximately 5% (1742.1N vs. 1822.9N) less total uplift force than that in Case 2. Compared with the RTWCs on the gable end, the ones connected to the interior trusses sustain higher uplift loads under the loading condition discussed. The maximum result in Case 1 occurs on the F2 RTWC with 309.9 N that is higher than the peak value in Case 2 which is 285.1N and occurs at the same location, i.e., 8% reduction. This reflects that breaking up the continuity on the gable end sheathing as well as the integrity of the structure will not increase the vulnerability of the RTWCs under uplift wind loads.

4.4 Effect of gable end truss stiffness/ different stiffness of the tress system

The introduction of the metal plate to connect wood trusses in the roofs of residential light-frame buildings in the mid-1950s significantly simplified the complicated system that was consisted of lumber rafters and board sheathing constructions before (Datin 2010). This change on the truss makes possible of its design to virtually any imaginable configuration and profile. This is the case, especially for the example of the gable end trusses, where they are most often built above the end wall saving the contractor the time and expense of field framing the end wall to match the roof slope (Gijinolli and Vogt 2007). However, it is imperative to remember these gable end trusses are parts of and must be incorporated into the design of the end wall to function integrally.

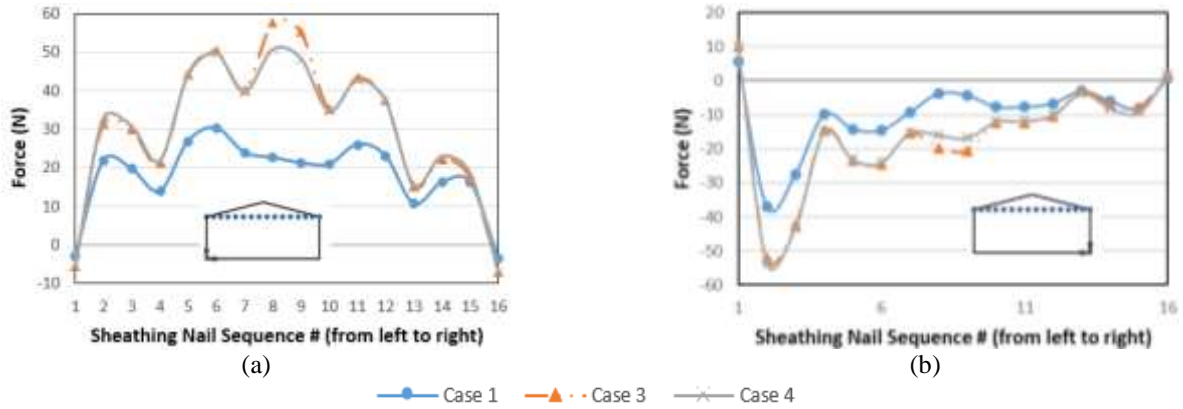


Fig. 12 Withdrawal force of gable sheathing nails at bottom chord: (a) left wall and (b) right wall

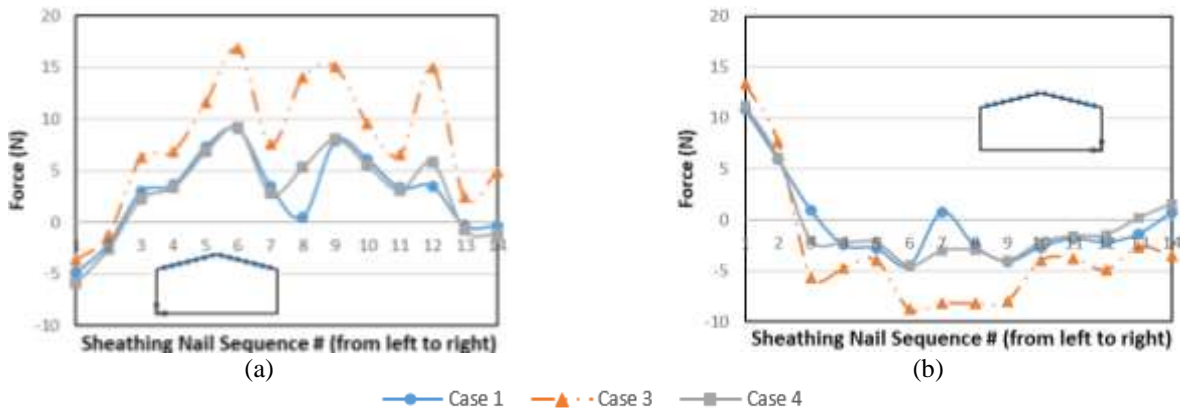


Fig. 13 Withdrawal force of gable sheathing nails at top chord: (a) left wall and (b) right wall

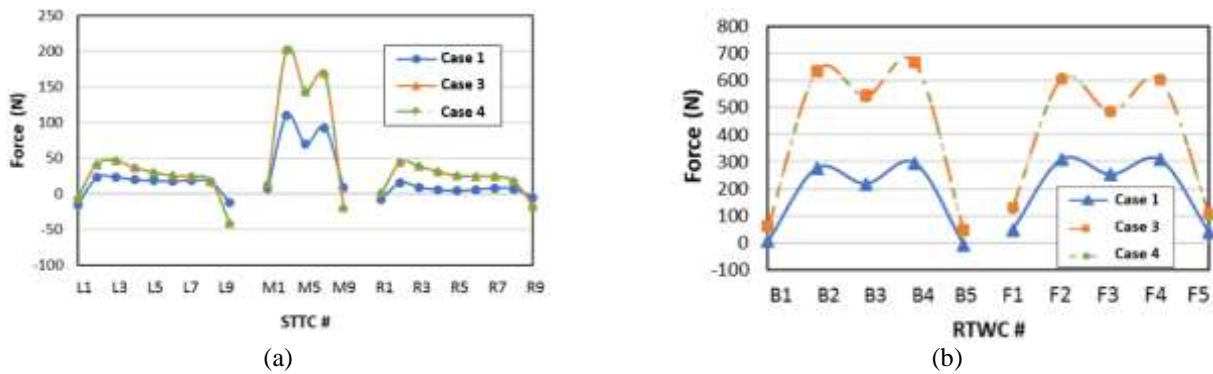


Fig. 14 Uplift force on: (a) STTCs and (b) RTWCs

The increased gable end stiffness is confirmed to attract more load and lead to the overloading of the STTCs on the roof as well as the removal of the roof sheathing due to this increased demand (Jacklin *et al.* 2014). However, this effect has yet to be studied in the analysis of the roof sheathing failure in terms of the withdrawal of the STTCs. Confusions also exist as which of these existing web configurations functions better. Reflecting these issues, three common truss shapes with the similar material quantity as shown in

Table 2 are selected as the gable end trusses in this section to study the effect of different truss types on the structural performance. The analysis on the withdrawal failure of the STTCs is also completed and will be presented later.

In the truss industry, the gable end frame is classified as the non-structural gable end frame having continuous support from the end wall along the entire span or the structural gable end frame with bearing at specific locations (Gjinolli and Vogt 2007). The former type is called so in that it is not designed

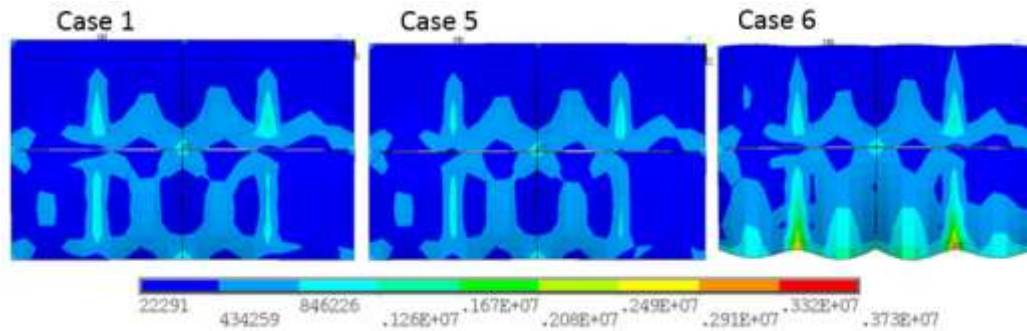


Fig. 15 VM comparison between roof sheathing (deformation scaler=50)

to transfer the horizontal load between side bearing walls along the span, and thus, the web members are oriented vertically and function as load carrying members only in vertical direction. As opposed to that, the latter is designed to carry loads over openings in the end wall containing both diagonal and vertical web members. As the capability of gable end frame to transfer loads from one bearing wall to another across the span could enhance the building stability, more analysis should be completed from this perspective by comparing the structural responses between constructions built with non-structural and structural gable end frames.

The building resistance to lateral loads is influenced by the gable end truss and provided by the sheathing, nail, and bracing, of which the first is the same for all the three types discussed whereas the rest two are different. The gable truss type is used for the two exterior trusses in the Case 1 model with five vertical webs and one sheathing nail on each web member in the middle. The Case 3 model is built on the fink style of end truss where four oblique webs are included without any sheathing nails on the web members but the sheathings are connected on the top and bottom chords. Compared with Case 3, the Case 4 model has one less web and one more sheathing nail in the queen style end truss adopted, where two oblique webs are symmetric about a vertical web with one sheathing nail in the middle. The effect of the truss shape on the gable end stiffness is illustrated through the withdrawal forces on the sheathing nails that are suspicious to fail, i.e., the ones at the bottom and top chord on the end wall.

The effect of the gable end truss type on the sheathing panel in terms of the force distribution can be seen in Fig. 11. There is a strong similarity in the pattern of the stress contours between Case 3 and Case 4. The stresses in Case 3, i.e., from 12649 to 574868 N/m² and 16388 to 445461 N/m² for the left and right wall, respectively, are close to the stress distribution in Case 4, i.e., from 13956 to 480460 and 11090 N/m² to 451475 N/m² for corresponding sheathing panel. The difference in the corresponding upper and lower limit of the two sets of stress ranges for Case 3 and Case 4 is as low as 1.3%. Opposed to that, the sheathing panels in Case 1 experience much lower force, which is evidenced by its stress range of 10156 to 342154 N/m² for the left side and 5927 to 29938 N/m² for the right side with the least absolute difference to Case 4 being 27%. One may conclude that the gable truss type with more webs and sheathing nails is stiffer than the fink and queen type.

The withdrawal forces on the sheathing nails cross the side walls demonstrate a similar variation along the same distance (Figs. 12 and 13). Whenever a sheathing nail connected to the bottom chord is lined up with the wall stud, e.g., nail #1, #4, and #7 in Fig. 12, the ability of the gable end sheathing panel to transfer loads to this nail is limited. For the sheathing nail at the bottom chord does not line up with the wall stud, as the case of nail #2 and #3 in Fig. 12, etc., the force transferred to withdraw the sheathing nail is notably larger, a similar observation noted by Jacklin *et al.* (2014) when investigating the load transfer on RTWCs by using the influence coefficient contours. This phenomenon is unable to detect in a simplified numerical model where either a single sheathing panel is modeled along the entire span (Datin 2010, Marin 2011), or beam elements are used to model the sheathing.

Of all the sheathing nails discussed in Figs. 12 and 13, the ones at the bottom chord on the left wall experience much higher withdrawal forces than the other three locations as shown in Fig. 12(a). This again reflects that the sheathing nails connected to the bottom chord are more vulnerable than the nails connected to the top chords on the gable end wall, and the effect of the truss shape on the building performance is well reflected in Fig. 12(a). Both the fink (Case 3) and queen (Case 4) trusses result in a similar load distribution over the gable end sheathing nails, differing by only 1% on average. Limited difference between the two cases occurs at the nails right beneath the roof ridge, i.e., nail #8 and #9, where the fink truss is higher by about 13%. The lower force on the queen truss is induced by adding the web sheathing nail through reducing the nailing tributary area, which is also witnessed in Fig. 13. Furthermore, adding more sheathing nails on the web is more effective than adding more webs to change the load distribution and reduce the local force on the gable end sheathing panel. Compared with the gable truss, the maximum value in the fink shape truss is almost doubled. As expected, with more components, the stiffer gable shape truss experienced the lowest demand for the sheathing nails attached and thus can withstand much more wind forces.

Fig. 14 takes another perspective of the uplift capacity of roof structure on the critical locations (defined in Fig. 5) including the STTCs and the RTWCs to examine the effect of gable end truss stiffness to the vulnerability of the structure. It is again found that the fink and queen truss shape models demonstrate very similar results on these

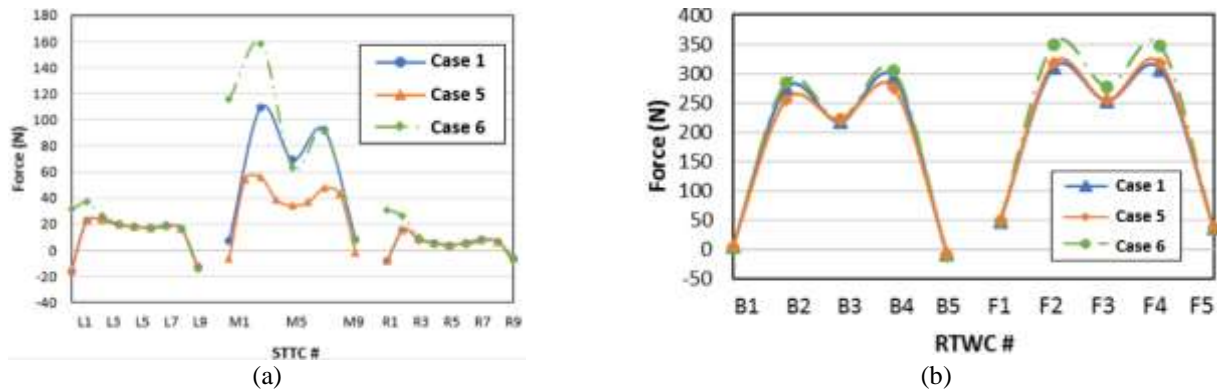


Fig. 16 Uplift force on: (a) STTCs and (b) RTWCs



Fig. 17 Same type of building nearby after Hurricane Charley (FEMA 2005)

critical locations and are higher than that of the gable truss shape model. This increased demand in the already weaker trusses would result in the overloading of the critical points for the light wood structures under wind loads after the removal of roof sheathing panels. The difference in the uplift forces of the STTCs on the front right roof sheathing panel is not that significant, especially on the edge nailing. However, for the uplift forces on the RTWCs, the maximum in the fink and queen truss shape models are over twice as large as that of the gable truss shape model.

4.5 Effect of STTC schedule

The roof sheathing failure was observed as the most common failure for wood-frame buildings under winds resulted from inadequate nailing to the underlying roof frame leading to discontinuous load path (van de Lindt *et al.* 2007, Prevatt *et al.* 2007). Even a single nail failure could often trigger the progressive failure of an entire roof. In other words, a proper installation of sheathing nails determines the performance of the roof structure as well as the entire structure, and a good command of the effect of nailing schedule is critical to the accuracy of the building performance prediction. Therefore, this section targets the effects of the STTC schedule on the uplift capacity of the roof structure by the comparisons between Cases 1, 5, and 6.

According to the US Census Bureau (2003), over 80% of the United States' residential structures in hurricane-prone areas were built before 1994, the year in which the code was upgraded due to Hurricane Andrew. Therefore, a

vast proportion of building stock was built on the old building provisions that specified the STTCs to be 6d smooth shank nails spaced at 6 in. / 12 in., e.g., the Florida Building Code (Dade County 1988). This nailing schedule is represented by the Case 1 model. In the building provision after 1994, the minimum requirement for the STTCs has been updated to be spaced at 6 in. / 6 in. (e.g., ICC 2007), and this schedule is analyzed by the Case 5 model. Additionally, other STTC schedules, due to the construction defects such as missing nails or the different requirement in the building codes from different geographic regions, are accounted for in the Case 6 model which also adopted in the FIU wind test model.

The VM stress distributions on the roof sheathing panels for Case 1, Case 5, and Case 6 are shown in Fig. 15. As the field nailing gets denser, the sheathing panels would become stiffer and are able to distribute the wind loads more evenly (Martin *et al.* 2011). By comparing the first two cases, this effect of nailing density is not significant for the current building configuration, where the maximum stress decreased by only 0.6% ($1.6E6$ N/m² of Case 1 and $3.73E6$ N/m² of Case 5) under the Case 5 nailing schedule at the same location. By comparing Case 1 and Case 6, one may note that without the edge nailing on the side walls, the Case 6 model with the fewest nailing experienced the highest stress of $3.73E6$ N/m² with an increment as large as 133.1% to that of the Case 1. The location of the maximum stress changed to the nail with the lowest nailing density.

Fig. 16 presents the effect of the roof sheathing nail schedule on the demand of the critical connections in the wood frame structures under the winds including the STTCs and the RTWCs. In Fig. 16(a), taking Case 5 as a benchmark, one can see that no matter whether the sheathing nails are missing in the field nailing such as Case 1, or with more nails missing in the edge nailing such as Case 6, the field sheathing nails are more sensitive to these changes than the nails on the edge. Also, the nail with less nailing density due to the nail missing around is as expected to have higher uplift force, e.g., L1 and R1. A similar trend is also observed in the uplift force on the RTWCs, where the one lines up with the field nailing is more sensitive to the roof sheathing nail schedule but with much smaller variations than that of the STTCs. One can conclude that using the sheathing nailing of higher density helps increase the capacity of both the roof sheathing panel and the RTWCs.

4.6 Effect of Opening

The pressurization caused by the internal pressure from the broken window or door is found to be an important factor in the structural failure. As shown in Fig. 17 that was taken after Hurricane Charley (FEMA 2005), one condominium without shutters lost most of its upper floor framing on the top unit; while the other one located two buildings away with a similar configuration but protected by shutters survived the storm relatively unscathed. It was the shutters that protected window and doors from debris, keeping the condo “enclosed” and preventing the generation of internal pressure pushing the roof to fail.

Reflecting on this dramatic failure of the roof structure contributed by the internal pressure, there has been active research on the quantification of internal pressures with various influencing parameters (Holmes 1979, Karava and Stathopoulos 2012, Pan *et al.* 2013). In contrast, the study is very rare focusing directly on the effect of the internal

pressure on the building response or the structural failure, especially on the decrease in the failure wind speed resulted from the increase of significant internal pressures. Furthermore, this information that relates the wind speed to the building damage is important for the damage and loss prediction for the insurance company. Thus, the effect of opening on the building performance is discussed in this section, and the failure part will be illustrated in a separate section later.

Generally speaking, the internal pressure would increase significantly due to the occurrence of the opening, together with the uplift external pressure pushing up the roof, leading to the higher stress intensity on the roof sheathing. However, how the wall reacts after the occurrence of opening is not fully studied. Therefore, the discussion here focuses on the stress on the wall with the opening instead of the roof as shown in Fig. 18. An obvious point to be made is that the presence of the opening will greatly reduce the probability that the front wall will be broken by extreme wind events. The peak pressure value of the part of the front wall presented has decreased by 72.9% from the 622557 N/m² in Case 1 to the 168412 N/m² in Case 7. As for the modeling method for the opening, whether the door is modeled in a separate sheathing panel or as a whole along the other sheathing does not have much effect to the stress prediction so that the peak stress of Case 1 and Case 8 occurs at the similar location with the similar value. Fig. 19 shows the uplift forces on the critical connections, i.e., the STTCs and the RTWCs, under the different opening conditions. As expected, the connections of either kind carry more uplift forces than the case without the opening. The peak forces on the STTCs and the RTWCs in Case 7 are more than doubled the peak values for Case 1. Again, the modeling method of the opening also has little effect on the capacity of the critical connection point.

One limitation of the current discussion is that, to be consistent with the FIU wind test model that had both the internal and external pressure data measured, the building model has only one equivalent opening, i.e., a door positioned in the center of the side wall. Thus, it is not representative of the typical residential structure. More analysis on building models with various opening conditions should be completed on this topic.

4.7 Effect of sheathing thickness

The effect of sheathing thickness, i.e., stiffness, is demonstrated in Figs. 20 and 21 by comparing the structural responses from models different in the sheathing thickness. As the thickness increased by 64.3% and 100% from the control case, the maximum VM stress in the sheathing of Cases 9 and 10 decreased by 31% and 78%, respectively. One may conclude that the sheathing capacity can be effectively increased by simply changing the thickness.

The capacity of the critical connectors is also influenced by the sheathing since it is the mechanism by which the loads are distributed. The sheathing panel facilitates the force distributions among the subcomponents of a structure, which has been found to be influenced by the relative stiffness of the sheathing and frame members to some

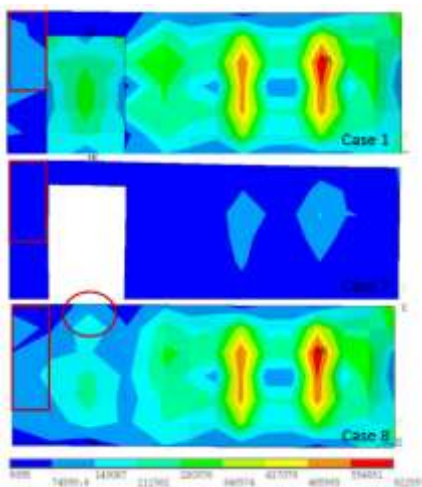


Fig. 18 VM stress comparison of the opening effect (deformation scaler=350)

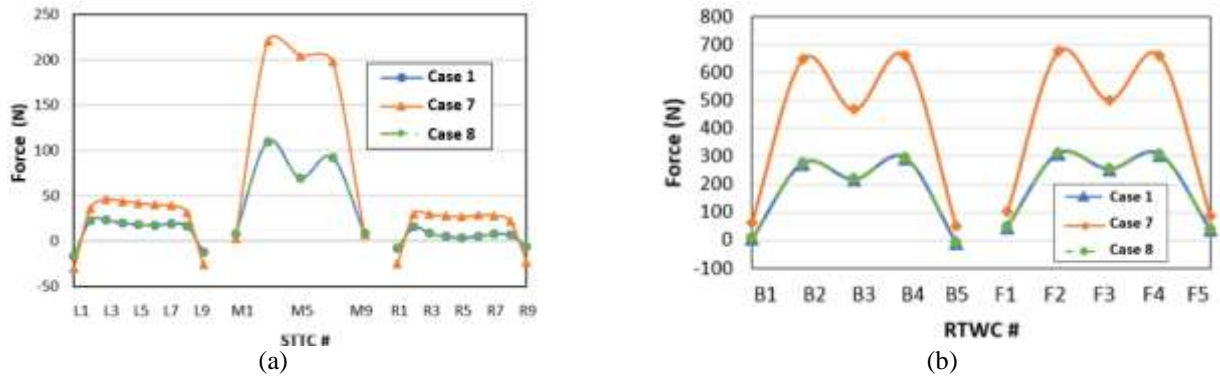


Fig. 19 Uplift force on: (a) STTCs and (b) RTWCs

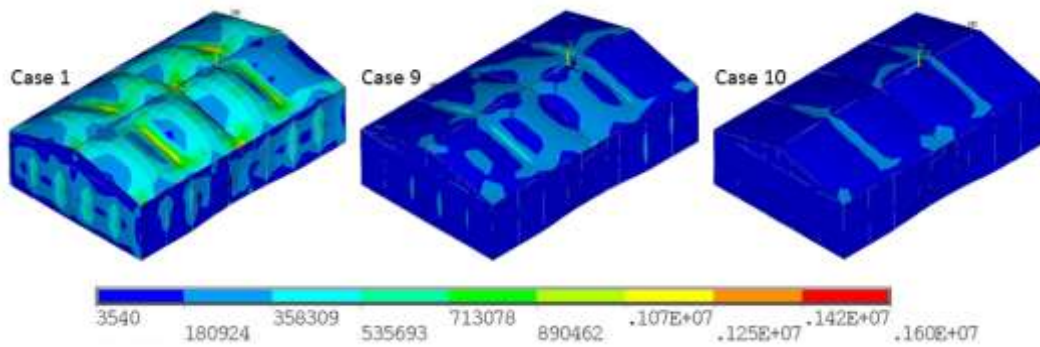


Fig. 20 VM stress comparison of the sheathing thickness (deformation scaler=60)

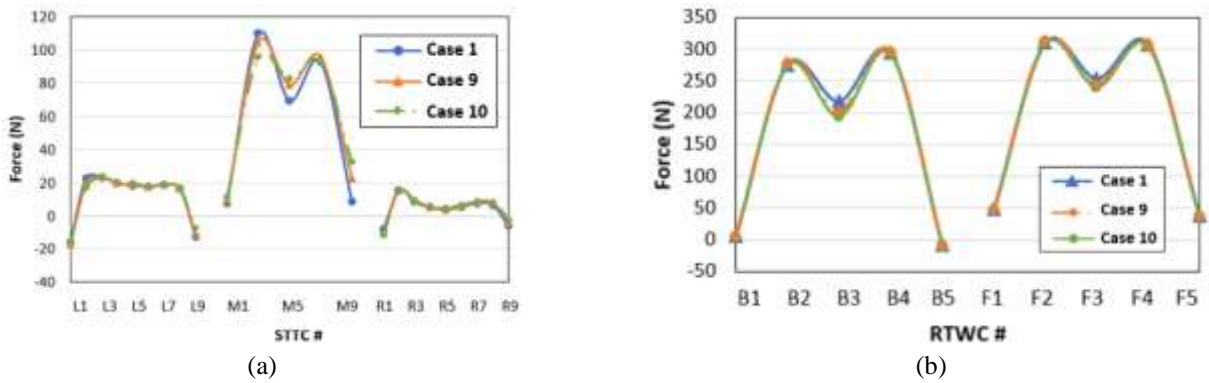


Fig. 21 Uplift force on: (a) STTCs and (b) RTWCs

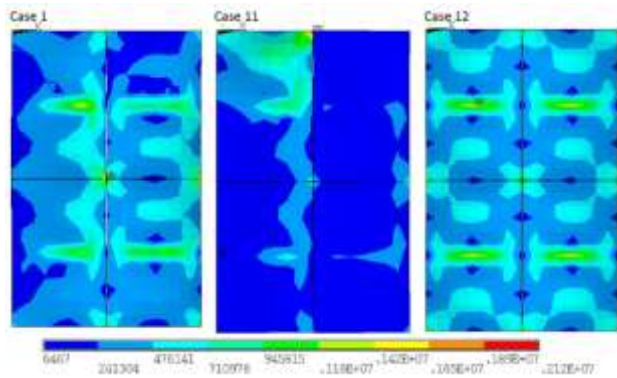


Fig. 22 VM stress comparison of load resolution (deformation scaler=50)

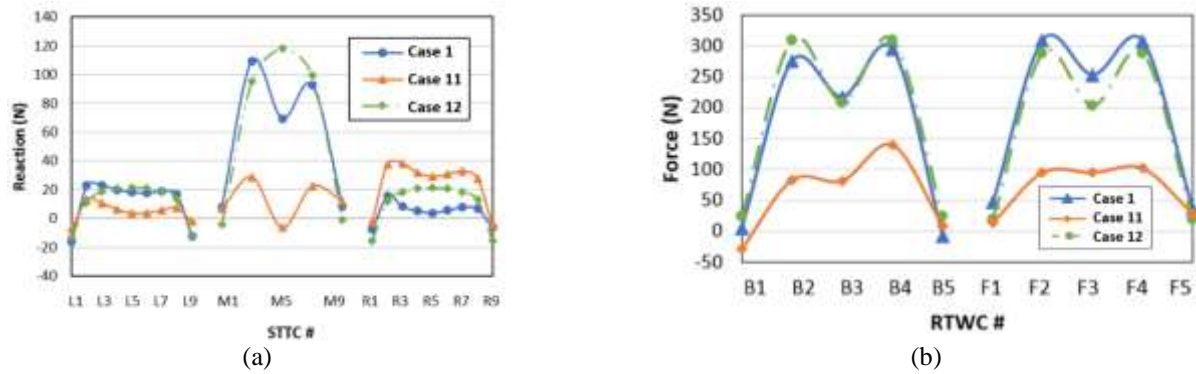


Fig. 23 Uplift force on: (a) STTCs and (b) RTWCs

extent (Cramer and Wolfe 1989). In Fig. 21(a), the uplift force distributed to the STTCs on the edge nailing (i.e., L1 to L9 and R1-R9 in Fig. 5) is barely affected by the sheathing stiffness, while for the field nailing (i.e., M1-M9), the force is more evenly distributed to the STTCs with stiffer sheathing but not to a large degree. For the RTWCs, Shivarudrappa and Nielson (2013) concluded that the low sheathing stiffness requiring a single RTWC to carry a higher share of the load applied directly to it. This applies especially on the RTWCs in the middle of the building (i.e., B3 and F3) where the sheathing panel gaps are located. Overall, a thicker roof sheathing panel would decrease the chance of both the sheathing panel itself and the critical connections to fail.

4.8 Effect of wind loading sources applied

The purpose of this section is to compare the effect of wind loading sources with different resolution on the building performance to gain further insight into the load sharing. The wind loading for the Cases 1 and 11 models are provided by a 1/4 large scale and 1/100 small scale building model measurements, respectively. The Case 12 model is applied with equivalent uniform pressures that match the realistic wind pressure distribution of Case 1 in terms of the global uplift force.

Fig. 22 shows the stress distribution on the roof sheathing panels subjected to each of the three wind loading sources discussed. One may observe that the wind loadings derived from small-scale model result in a similar stress distribution pattern with that under the loads from the large-scale model but with discrepancies on the magnitude especially near the roof's leading edges, roof corner, and roof ridges. This indicates that the small-scale wind tunnel tests cannot reproduce the peak pressures on the roof regions under conical vortices or separation bubbles attributed to the missing of large eddies, a characteristic has been noted elsewhere (e.g., Meecham *et al.* 1991.; Hoxey *et al.* 1998) by comparing the pressure coefficients from the full-scale and wind tunnel test measurements. For the uniform pressure results, the stress on the roof sheathing achieves the peak value around the field nailing implying that the capacity of the sheathing is influenced by the nailing density.

Fig. 23 presents the comparisons of the uplift force on the STTCs and the RTWCs under the three loading sources. Based on the connectors examined, the wind pressures from the small-scale model underestimated the maximum uplift forces, and thus, it is questionable that if such a loading is sufficient to analyze the structural behavior and predict the failure state of full scale buildings. It is noteworthy that the extent of the underestimation due to the scaling effect may not be as large as it is shown in the figure, since even measured in wind tunnel on the model with the same scale, the pressures can be different from laboratory to laboratory, e.g., the international round-robin set of wind tunnel tests of a low-rise structure conducted at six reputable laboratories (Fritz *et al.* 2008). For the equivalent uniform pressure, it is interesting to find that even without considering the wind incident direction, the uplift forces on the critical connectors examined exhibit similar results. Additionally, the peak values are higher than that of the Case 1 results, indicating the equivalent uniform pressure can be sufficient to create a similar behavior to the realistic pressure distribution under certain circumstances.

5. Summary of results

To give a whole picture of the influence from all the parameters studied, the maximum VM stress for the entire building surface of each case is summarized in Fig. 24. Besides, further analysis is conducted on the first failure wind speed and the location of critical connections as shown in Fig. 25. These two indicators shed lights directly on the question of the influence of the geometric parameters and loading resolution on the building performance. This connection result together with the sheathing response provides a better understanding of the load sharing in the light-frame wood house in overall and localized scale.

Breaking up the sheathing continuity (i.e., from Case 1 to Case 2) at the gable end does not change much of the building performance, causing only 1% decrease in the sheathing demand and 4% increase in connection demand. The effect of gable end truss stiffness determined by the truss shape is apparent on the sheathing behavior with the maximum stress increased by over 90% in both Cases 3 and 4 compared to the gable type Case 1 model. However, there is essentially

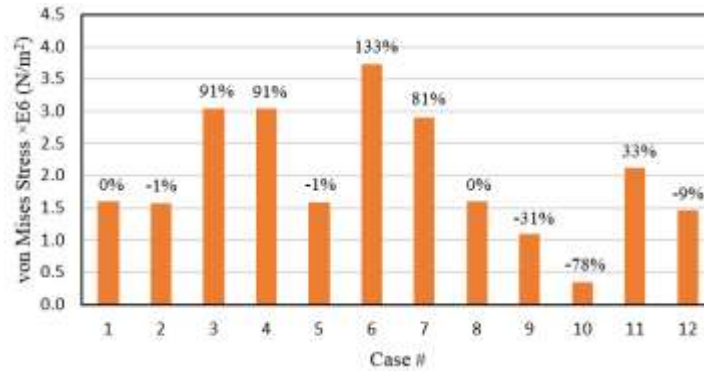


Fig. 24 Maximum VM stress of each case (with percentage difference to Case 1)

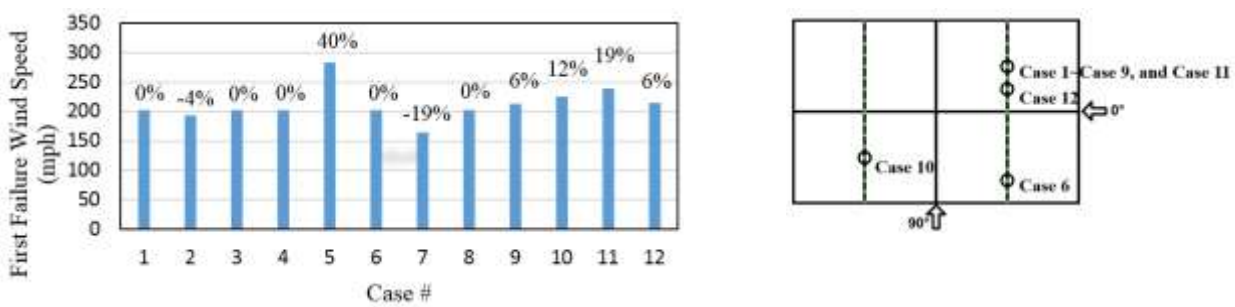


Fig. 25 First failure wind speed (with percentage difference to Case 1) and location of each case

no notable difference between the demand for the critical connections under the different truss shapes. The differences between Cases 1, 5, and 6 are significant, which are conducted to compare the effect of the sheathing nail schedule to the building vulnerability. With more field nails, although the resulted peak sheathing stress is almost equal, there is a pronounced increment by as large as 40% in the highest wind speed that the building can take. Opposed to that, with missing nails on the roof edge, the sheathing panels are at a higher risk of failure, while the force of the sheathing nails barely changes. The effect of the opening is significant as demonstrated in Case 7 that the sheathing is subjected to over 100% higher forces, and the highest wind speed plummets 19% from 202 mph to 164 mph suggesting that the building resistance to the winds has been greatly weakened. As for the way that the door is modeled, it has little to no effect on both the sheathing and nail response as shown in the results of Case 8. Thus, one may reasonably conclude that there is no need to model the opening such as the door and the window in a separate sheathing panel for the enclosed condition when analyzing the building performance under winds. By comparing the results of Cases 1, 9, and 10, the benefit of having the thicker sheathing is obvious in enhancing the capacities of both the sheathing and critical connections.

For the wind loading of three different resolutions, the one measured from small-scale building model leads to a higher peak stress on the sheathing panel by 33% and an increase of 19% in the first failure wind speed compared with the results under the wind loads derived from the

large-scale model. This suggests that using the wind pressure data from small-scale wind tunnel tests such as the NIST database is conservative for the sheathing design but unconservative for the design of critical connections which govern the vulnerability of buildings in extreme wind events. The Case 12 model which is subjected to the uniform loading underestimates the maximum force on both the sheathing panel and the STTCs.

The location of the first failure STTC partially reflects the load paths and distribution in the structure. Most of the cases, i.e., Cases 2 - 9, and 11, fail at the same place with the control case, Case 1, as shown in Fig. 25, indicating the failure sequence to some extent. Exceptions exist in Cases 6, 10, and 12. The first STTC to fail in Case 6 that has missing nails on the roof edges is on the front roof sheathing, which is different from the control case, emphasizing the significant influence of the nails schedule, especially of the edge nailing, on the load paths of the structure. It is also noted that failure beginning from the front right roof sheathing in Case 6 is consistent with the phenomenon observed from the FIU destructive wind test, which further verified the modeling methodology in the failure stage. From the different failure locations of Case 10 compared to the control case, it is interesting to find that the load sharing is more sensitive to the sheathing thickness than many other building configurations by changing the relative stiffness of sheathing to framing and connectors. As for Case 12, the first failure location subjected to the uniform loading is reasonably different from that of the control case under realistic wind loading.

6. Conclusions

This study aims to enhance the understanding of the effect of parameters that have great influence on the load paths and especially are critical to the failure of older buildings. This is done by conducting a parametric study on a 3D FE building model subjected to various geometric and loading scenarios such as the gable end sheathing continuity, the gable end truss stiffness, the STTC schedule, the opening condition, etc. It is noteworthy that the coupling effect between the parameters is not studied, and the further work should examine and quantify this effect on the building vulnerability. The conclusions are formed on the basis of and limited to the building models described and load cases conducted herein. The extension of these conclusions is expected in the future study to serve a better estimation on the performance of the existing building stock under high winds, enable the application of proper mitigation techniques, and guide the future constructions. Specific conclusions are drawn as follows:

- Breaking up the sheathing continuity on the gable end changes the load sharing and even the direction of the way that loads are distributed, but it does not much weaken the structure. The structural integrity is compensated due to the higher nailing density by adding extra sheathing nails at the breakup joint according to the same nailing schedule. For the model studied, the peak demand of the RTWC and the sheathing nail decreased 8% and 54.3%, respectively, after breaking up the sheathing continuity due to the higher nail density at the gable end.

- The truss shape that has more webs and nails at the gable end greatly reduce the demand of the sheathing nails and RTWCs as high as 50% but has little effect to the failure of STTCs. The fink and queen shape trusses with the same components quantity exhibit similar performance.

- The roof nailing schedule strongly influences the resistance of the building especially the roof field nails to winds. Missing nails at the roof edge will change the load sharing and lead to a different progressive failure of the house.

- The occurrence of opening on the wall in a building model that has only one door opening on one of the side walls decreases the load carried by that wall and increases the building vulnerability to winds by 20% in terms of first failure wind speed. No specific modeling is needed on the door or window for the enclosed condition in the analysis of the building performance to the wind.

- Overall, one of the most efficient ways to mitigate the failure of the light-frame wood structure to wind loading is to be installing extra sheathing nails, especially on the field nailing. Meanwhile, choosing a thicker sheathing panel also helps in building a stronger house. Of all the geometric parameters examined, a missing of nails leads to the worst case and should be avoided in the construction.

The possible unconservative building design can be induced by using the wind loads from the small-scale wind tunnel tests. Uniform loading is not sufficient to reflect the load sharing and building behavior under wind load distribution.

Acknowledgments

This work is partially supported by the NSF project No. CMMI-1233991 and Louisiana State University under the Economic Development Assistantship for the first author. The contents of the paper reflect only the views of the authors. These supports are greatly appreciated.

References

- Ahmad, S. and Kumar, K. (2002), "Effect of geometry on wind pressures on low-rise hip roof buildings", *J. Wind Eng. Ind. Aerod.*, **90** (7), 755-779. [https://doi.org/10.1016/S0167-6105\(02\)00152-6](https://doi.org/10.1016/S0167-6105(02)00152-6).
- ASCE 7-10. (2010), "Minimum design loads for buildings and other structures", Reston (Virginia): American Society of Civil Engineers.
- Asiz, A., Chui, Y.H., Zhou, L. and Smith, I. (2009), "Development of advanced system design procedure in Canadian Wood Design Standard. Final Report", Natural Resources Canada, Ottawa.
- Cope A. (2004), "Predicting the vulnerability of typical residential buildings to hurricane damage", Ph.D. Dissertation, University of Florida, Gainesville, FL.
- Cramer, S.M. and Wolfe, R.W. (1989), "Load-distribution model for light frame wood roof assemblies", *J. Struct. Eng.*, **115**(10), 2603-2616. [https://doi.org/10.1061/\(ASCE\)0733-9445\(1989\)115:10\(2603\)](https://doi.org/10.1061/(ASCE)0733-9445(1989)115:10(2603))
- Dade County. (1988), "South Florida Building Code", Dade County Board of County Commissioners, Miami, Dade County, FL.
- Datin, P.L. (2010), "Structural load paths in low-rise, wood-framed structures", Ph.D. Thesis. Department of Civil and Coastal Engineering, University of Florida, Gainesville, FL.
- Dao, T. and van de Lindt, J. (2008), "New nonlinear roof sheathing fastener model for use in finite-element wind load applications", *J. Struct. Eng.*, **134** (10), 1668-1674. [https://doi.org/10.1061/\(ASCE\)0733-9445\(2008\)134:10\(1668\)](https://doi.org/10.1061/(ASCE)0733-9445(2008)134:10(1668)).
- Dickers, R.D., Marshall, R.D. and Thom, H.C.S. (1970), "Hurricane Camille—August 1969: A survey of structural damage along the Mississippi Gulf Coast", National Bureau of Standards, Washington, DC.
- Pan, F., Cai, C.S., Zhang, W. and Kong, B. (2014), "Refined damage prediction of low-rise building envelope under high wind load", *Wind Struct.*, **18**(6), 669-691. <https://doi.org/10.12989/was.2014.18.6.669>.
- FEMA. (2005), "Hurricane Charley in Florida, Report #488", Washington, DC: Federal Emergency Management Agency.
- FEMA. (2006), "Summary report on building performance, Report #548", Washington, DC: Federal Emergency Management Agency.
- Fischer, C. and Kasal, B. (2009), "Analysis of light-frame, low-rise buildings under simulated lateral wind loads", *Wind and Structures*, 10.12989/was.2009.12.2.089, 89-101. Online publication date: 25-Mar-2009.
- Fritz, W. P., Bienkiewicz, B., Cui, B. and Flamand, O. (2008), "International comparison of wind tunnel estimates of wind effects on low-rise buildings: Test-related uncertainties", *J. Struct. Eng.*, **134**(12), 1887-1890. [https://doi.org/10.1061/\(ASCE\)0733-9445\(2008\)134:12\(1887\)](https://doi.org/10.1061/(ASCE)0733-9445(2008)134:12(1887)).
- Gjinolli, G. and Vogt, J. (2007), Wood Truss Gable End Frames, *Structure magazine*, Aug.
- He, J., Pan, F. and Cai, C.S. (2017), "A review of wood-frame low-rise building performance study under hurricane winds", *Eng. Struct.*, **141**, 512-529. <https://doi.org/10.1016/j.engstruct.2017.03.036>.

- He, J., Pan, F. and Cai, C.S. (2018a), "Assessment of ASCE 7-10 for wind effects on low-rise wood frame buildings with database-assisted design methodology", *Wind Struct.*, **27**(3), 163-173. <https://doi.org/10.12989/was.2018.27.3.163>
- He, J., Pan, F., and Cai, C.S., Habte, F. and Chowdhury, A. (2018b), "Finite-element modeling framework for predicting realistic responses of light-frame low-rise buildings under wind loads", *Eng. Struct.*, **164**(1), 53-69. <https://doi.org/10.1016/j.engstruct.2018.01.034>.
- He, J., Pan, F., Cai, C.S., Habte, F. and Chowdhury, A. (2018c), "New DAD application: progressive failure of low-rise timber buildings under extreme wind events", *J. Wind Eng. Ind. Aerod.*, under second review.
- Ho, T.C.E., Surry, D., Morrish, D. and Kopp, G.A. (2005), "The UWO contribution to the NIST aerodynamic database for wind loads on low buildings: Part I. Archiving format and basic aerodynamic data", *J. Wind Eng. Ind. Aerod.*, **93**(1), 1-30. <https://doi.org/10.1016/j.jweia.2004.07.006>.
- Holmes, J.D. (1979), "Mean and fluctuating internal pressure induced by wind", *Proceedings of the 5th Int. Conf. on Wind Engineering*, Fort Collins, Colo. 435-450.
- Hoxey, R.P., Robertson, A. and Short, L. (1998), "The role of corner vortices in the design of structures", *Struct. Eng. Int.*, **1**(98), 50-55.
- ICC. (2007), "Florida Building Code", Building, International Code Council, Inc., Falls Church, VA.
- Jacklin, R.B., El Damatty, A.A. and Dessouki, A.A. (2014), "Finite-element modeling of a light-framed wood roof structure", *Wind Struct.*, **19**(6), 602-621. <https://doi.org/10.12989/was.2014.19.6.603>.
- Karava, P. and Stathopoulos, T. (2012), "Wind-induced internal pressures in buildings with large façade openings", *J. Eng. Mech.*, **138**(4), 358-370. [https://doi.org/10.1061/\(ASCE\)EM.1943-7889.0000296](https://doi.org/10.1061/(ASCE)EM.1943-7889.0000296).
- Malone, B., Miller, T. and Gupta, R. (2013), "Gravity and wind load path analysis of a light-frame and a traditional timber frame building", *J. Archit. Eng.*, [https://doi.org/10.1061/\(ASCE\)AE.1943-5568.0000136](https://doi.org/10.1061/(ASCE)AE.1943-5568.0000136)
- Martin, K.G., Gupta, R., Prevatt, D.O., Datin, P.L. and van de Lindt, J.W. (2011), "Modeling system effects and structural load paths in a wood-framed structure", *J. Archit. Eng.*, **17**(4), 134-143.1 [https://doi.org/10.1061/\(ASCE\)AE.1943-5568.0000045](https://doi.org/10.1061/(ASCE)AE.1943-5568.0000045).
- Meecham, D., Surry, D. and Davenport, A.G. (1991), "The magnitude and distribution of wind-induced pressures on hip and gable roofs", *J. Wind Eng. Ind. Aerod.*, **38**(2-3), 257-272. [https://doi.org/10.1016/0167-6105\(91\)90046-Y](https://doi.org/10.1016/0167-6105(91)90046-Y).
- Mensah, A.F., Datin, P.L., Prevatt, D.O., Gupta, R. and van de Lindt, J.W. (2011), "Database-assisted design methodology to predict wind-induced structural behavior of a light-framed wood building", *Eng. Struct.*, **33**(2), 674-684. <https://doi.org/10.1016/j.engstruct.2010.11.028>.
- Pan, F., Cai, C. and Zhang, W. (2013), "Wind-induced internal pressures of buildings with multiple openings", *J. Eng. Mech.*, **10**, 376-385. [https://doi.org/10.1061/\(ASCE\)EM.1943-7889.0000464](https://doi.org/10.1061/(ASCE)EM.1943-7889.0000464).
- Pfretzschner, K., Gupta, R. and Miller, T. (2014), "Practical modeling for wind load paths in a realistic light-frame wood house", *J. Perform. Constr. Fac.*, **28**(3), [https://doi.org/10.1061/\(ASCE\)CF.1943-5509.0000448](https://doi.org/10.1061/(ASCE)CF.1943-5509.0000448).
- Prevatt, D.O. and Datin, P.L. (2007), "Wind uplift reactions at roof-to-wall connections of wood-framed gable roof assembly", SC Sea Grant Project Number: R191.
- Roueche, D.B., Prevatt, D.O., Haan, F.L. and Datin, P.L. (2015), "An estimate of tornado loads on a wood-frame building using database-assisted design methodology", *J. Wind Eng. Ind. Aerod.*, **138**, 27-35. <https://doi.org/10.1016/j.jweia.2014.11.011>.
- Satheeskumar, N., Henderson, D., Ginger, J. and Wang, C. (2016), "Wind uplift strength capacity variation in roof-to-wall connections of timber-framed houses", *J. Archit. Eng.*, **22**(2), [https://doi.org/10.1061/\(ASCE\)AE.1943-5568.0000204](https://doi.org/10.1061/(ASCE)AE.1943-5568.0000204).
- Shivarudrappa, R. and Nielson, B. (2013), "Sensitivity of load distribution in light-framed wood roof systems due to typical modeling parameters", *J. Perform. Constr. Fac.*, **27**(3), [https://doi.org/10.1061/\(ASCE\)CF.1943-5509.0000323](https://doi.org/10.1061/(ASCE)CF.1943-5509.0000323).
- Sparks, P.R. (1991), "Hurricane Hugo in perspective", NIST Special Publication 820, National Institute of Standards & Technology, 29-37.
- Tieleman, H.W. (1996), "Model/full scale comparison of pressures on the roof of the TTU experimental building", *J. Wind Eng. Ind. Aerod.*, **65**(1-3), 133-142. [https://doi.org/10.1016/S0167-6105\(97\)00030-5](https://doi.org/10.1016/S0167-6105(97)00030-5).
- Tieleman, H.W. (2003), "Wind tunnel simulation of wind loading on low rise structures: A review", *J. Wind Eng. Ind. Aerod.*, **91**(12-15), 1627-1649. <https://doi.org/10.1016/j.jweia.2003.09.021>.
- US Census Bureau. (2003), "Census of population and housing (2000)", U.S. Dept. of Commerce, Economics and Statistics Administration, Washington, D.C.
- US Census Bureau. (2007), "2007 Population Estimates", US Dept. of Commerce, Economics and Statistics Administration, Washington, D.C., Accessed 9/16/2009 from factfinder.census.gov.
- van de Lindt, J.W., Graettinger, A., Gupta, R., Skaggs, T., Pryor, S., and Fridley, K.J. (2007), "Performance of wood-frame structures during Hurricane Katrina", *J. Perform. Constr. Fac.*, **21**(2), 108-116. [https://doi.org/10.1061/\(ASCE\)0887-3828\(2007\)21:2\(108\)](https://doi.org/10.1061/(ASCE)0887-3828(2007)21:2(108)).
- Wilson, S. and Rischetti, T. (2010), "Coastline population trends in the United States: 1960 to 2008", U.S. Census Bureau.
- Wolfe, R.W. and McCarthy, M. (1989), "Structural performance of light-frame roof assemblies: I. Truss assemblies with high truss stiffness variability", FPL-RP-492, Forest Products Laboratory, Madison, WI. 1989.
- Wolfe, R.W. and LaBissoniere, T. (1991), "Structural Performance of Light-Frame Roof Assemblies II. Conventional Truss Assemblies", Forrester Products Laboratory, Research Paper: FPL-RP-499

AD